

Article

Phase Formation, Microstructure, and Magnetic Properties of Nd_{14.5}Fe_{79.3}B_{6.2} Melt-Spun Ribbons with Different Ce and Y Substitutions

Qingjin Ke ¹, Feilong Dai ¹, Shengxi Li ¹, Maohua Rong ^{1,2,*}, Qingrong Yao ^{1,2} and Jiang Wang ^{1,2,*}

¹ Guangxi Key Laboratory of Information Materials, School of Materials Science and Engineering, Guilin University of Electronic Technology, Guilin 541004, China; keqingjin2021@163.com (Q.K.); dfldeyouxiang123@163.com (F.D.); lxx1027297604@163.com (S.L.); qingry96@guet.edu.cn (Q.Y.)

² Engineering Research Center of Electronic Information Materials and Devices, Ministry of Education, Guilin University of Electronic Technology, Guilin 541004, China

* Correspondence: rongmh124@guet.edu.cn (M.R.); waj124@guet.edu.cn (J.W.)

Abstract: Phase formation and microstructure of (Nd_{1-2x}Ce_xY_x)_{14.5}Fe_{79.3}B_{6.2} (x = 0.05, 0.10, 0.15, 0.20, 0.25) alloys were studied experimentally. The results reveal that (Nd_{1-2x}Ce_xY_x)_{14.5}Fe_{79.3}B_{6.2} annealed alloys show (NdCeY)₂Fe₁₄B phase with the tetragonal Nd₂Fe₁₄B-typed structure (space group P4₂/mnm) and rich-RE (α-Nd) phase, while (Nd_{1-2x}Ce_xY_x)_{14.5}Fe_{79.3}B_{6.2} ribbons prepared by melt-spun technology are composed of (NdCeY)₂Fe₁₄B phase, α-Nd phase and α-Fe phase, except for the ribbon with x = 0.25, which consists of additional CeFe₂ phase. On the other hand, magnetic properties of (Nd_{1-2x}Ce_xY_x)_{14.5}Fe_{79.3}B_{6.2} melt-spun ribbons were measured by a vibrating sample magnetometer (VSM). The measured results show that the remanence (B_r) and the coercivity (H_{cj}) of the melt-spun ribbons decrease with the increase of Ce and Y substitutions, while the maximum magnetic energy product ((BH)_{max}) of the ribbons decreases and then increases. The tendency of magnetic properties of the ribbons could result from the co-substitution of Ce and Y for Nd in Nd₂Fe₁₄B phase and different phase constitutions. It was found that the H_{cj} of the ribbon with x = 0.20 is relatively high to be 9.01 kOe, while the (BH)_{max} of the ribbon with x = 0.25 still reaches to be 9.06 MGOe. It suggests that magnetic properties of Nd-Fe-B ribbons with Ce and Y co-substitution could be tunable through alloy composition and phase formation to fabricate novel Nd-Fe-B magnets with low costs and high performance.

Keywords: Nd-Ce-Y-Fe-B; melt-spun ribbon; phase structure; magnetic properties



Citation: Ke, Q.; Dai, F.; Li, S.; Rong, M.; Yao, Q.; Wang, J. Phase Formation, Microstructure, and Magnetic Properties of Nd_{14.5}Fe_{79.3}B_{6.2} Melt-Spun Ribbons with Different Ce and Y Substitutions. *Materials* **2021**, *14*, 3992. <https://doi.org/10.3390/ma14143992>

Academic Editor: Joan-Josep Suñol

Received: 31 May 2021

Accepted: 14 July 2021

Published: 16 July 2021

Publisher's Note: MDPI stays neutral with regard to jurisdictional claims in published maps and institutional affiliations.



Copyright: © 2021 by the authors. Licensee MDPI, Basel, Switzerland. This article is an open access article distributed under the terms and conditions of the Creative Commons Attribution (CC BY) license (<https://creativecommons.org/licenses/by/4.0/>).

1. Introduction

Since discovered in 1983, Nd-Fe-B magnets as outstanding magnetic materials have been used intensively in variously industrial applications such as motors of electric/hybrid vehicles and electric generators [1–3]. In general, Nd-Fe-B magnets would improve greatly their coercivity through the addition of the low-abundant and expensive rare earth (RE) metals Dy and Tb. With the emerging applications for the purpose of the electronic industry, the demand for Nd-Fe-B magnets is increasing rapidly, which causes the excessive use of rare earth metals Nd, Pr, Dy, and Tb. Meanwhile, the high-abundant and cheap rare earth metals La, Ce, and Y were not used effectively in the production of Nd-Fe-B magnets. Therefore, the integrated utilization of rare earth metals in Nd-Fe-B magnets is a promising way to achieve the sustainable development of Nd-Fe-B magnets [4–34]. However, the magnetic properties of Nd-Fe-B magnets with La, Ce, and Y have deteriorated unavoidably through the traditional fabrication technology because intrinsic magnetic properties of La₂Fe₁₄B, Ce₂Fe₁₄B, and Y₂Fe₁₄B phases are inferior to those of Nd₂Fe₁₄B, Dy₂Fe₁₄B, and Tb₂Fe₁₄B phases [35]. Recently, different fabrication technologies (e.g., double main phase method, dual alloy method, and grain boundary diffusion method) and microstructure

optimization (e.g., grain boundary restructure) were developed to improve magnetic properties of Nd-Fe-B magnets with La, Ce, and Y [6–34].

In particular, the magnetic performance of Y and/or Ce substituted Nd-Fe-B alloys were investigated in the literature [26–34]. Chen et al. [26] reported that $\text{Nd}_{9-x}\text{Y}_x\text{Fe}_{72}\text{Ti}_2\text{Zr}_2\text{B}_{15}$ nanocomposite ribbons exhibited high coercivity (923.4 kA/m). Fan et al. [30] found that Y substituted Nd-Ce-Fe-B sintered magnets show special core-shell microstructure characteristics with Y-rich core and Nd-rich shell, resulting in the improvement of the coercivity and the thermal stability of magnets. Zheng et al. [32] studied magnetic properties of $(\text{Nd}_{1-x}\text{Y}_x)_{14.5}\text{Fe}_{\text{bal}}\text{B}_6\text{Co}_{0.2}\text{Al}_1\text{Cu}_{0.15}$ melt-spun ribbons. Zhang et al. [34] investigated phase constituent, microstructure, and magnetic properties of $\text{Nd}_{12-x}\text{Y}_x\text{Fe}_{81}\text{B}_6\text{Nb}$ melt-spun ribbons. The results [32,34] show that the magnetic properties of ribbons reduce gradually with increasing Y content. Liao et al. [33] studied the effect of element distribution on the magnetic performance of (PrNd)-(Y_{10-x}Ce_x)-Fe-B sintered magnets. The remarkable increase of the coercivity of magnets with $x = 2$ indicated that Y-Ce co-substitution could improve the magnetic properties of Nd-Fe-B magnets. The experimental results [26–34] indicate the significant effect of alloy composition, microstructure, and fabrication technology on the magnetic properties of Nd-Fe-B alloys with Ce and/or Y substitution. In order to understand further the effect of phase formation and microstructure on magnetic properties of Nd-Fe-B alloys with Ce and Y co-substitution, phase structure, microstructure, and magnetic properties of $(\text{Nd}_{1-2x}\text{Ce}_x\text{Y}_x)_{14.5}\text{Fe}_{79.3}\text{B}_{6.2}$ alloys were studied experimentally in this work.

2. Experimental Procedure

Pure bulk Nd, Ce, Fe and B (99.99% purity) were used to prepare $(\text{Nd}_{1-2x}\text{Ce}_x\text{Y}_x)_{14.5}\text{Fe}_{79.3}\text{B}_{6.2}$ ($x = 0.05, 0.10, 0.15, 0.20, 0.25$) alloys by arc-melting method. After being melted four times, alloy samples were sealed in vacuum quartz tubes to be annealed at 1173 K for 360 h. The ribbons were obtained by induction melting the annealed alloys and then ejecting melts through the orifice (orifice diameter about 0.8–1.0 mm) of quartz tubes onto the copper wheel surface with wheel speeds of 20–30 m/s.

The crystal structures of the formed phases in the annealed alloys and melt-spun ribbons were examined using X-ray powder diffraction (XRD, PLXcel 3D, PANalytical, Almelo, the Netherlands, Cu K_α radiation). The microstructure of the annealed alloys was tested by scanning electron microscopy (SEM, Quanta FEG-450, FEI, Hillsboro, OR, USA). Magnetic measurements of the ribbons were carried out using the Lakeshore VSM (Model 7400 740H, Lake Shore Cryotronics, Westerville, OH, USA) at room temperature. The demagnetization correction of the ribbons was not considered because the applied magnetic field is parallel to the plane of the ribbons during the magnetic measurements.

3. Results and Discussion

3.1. Phase Structure and Microstructure

Figure 1 shows the XRD patterns of $(\text{Nd}_{1-2x}\text{Ce}_x\text{Y}_x)_{14.5}\text{Fe}_{79.3}\text{B}_{6.2}$ alloys annealed at 1173 K for 360 h. In Figure 1a, all alloys contain the $(\text{NdCeY})_2\text{Fe}_{14}\text{B}$ phase with isotropic $\text{Nd}_2\text{Fe}_{14}\text{B}$ structure (space group $P4_2/mnm$) and rich-RE (α -Nd) phase. Figure 1b presents the local XRD patterns of $(\text{Nd}_{1-2x}\text{Ce}_x\text{Y}_x)_{14.5}\text{Fe}_{79.3}\text{B}_{6.2}$ annealed alloys. The diffraction peak around 30° is belonged to the rich-RE (α -Nd) phase, while the weak diffraction peak at 45.4° confirms that the α -Fe phase was not formed. It is evident in Figure 1b that the diffraction peaks of the $(\text{NdCeY})_2\text{Fe}_{14}\text{B}$ phase shift slightly to the direction of high angle with the increase of Ce and Y substitutions because the lattice constants of $\text{Y}_2\text{Fe}_{14}\text{B}$ ($a = 0.8757$ nm, $c = 1.2026$ nm) and $\text{Ce}_2\text{Fe}_{14}\text{B}$ ($a = 0.8726$ nm, $c = 1.2057$ nm) are smaller than those of $\text{Nd}_2\text{Fe}_{14}\text{B}$ ($a = 0.8792$ nm, $c = 1.2177$ nm) [35]. It suggests that Ce and Y atoms replace Nd atoms in the lattice of the $\text{Nd}_2\text{Fe}_{14}\text{B}$ phase, leading to shifting diffraction peaks to the direction of high angles according to the Bragg equation [32].

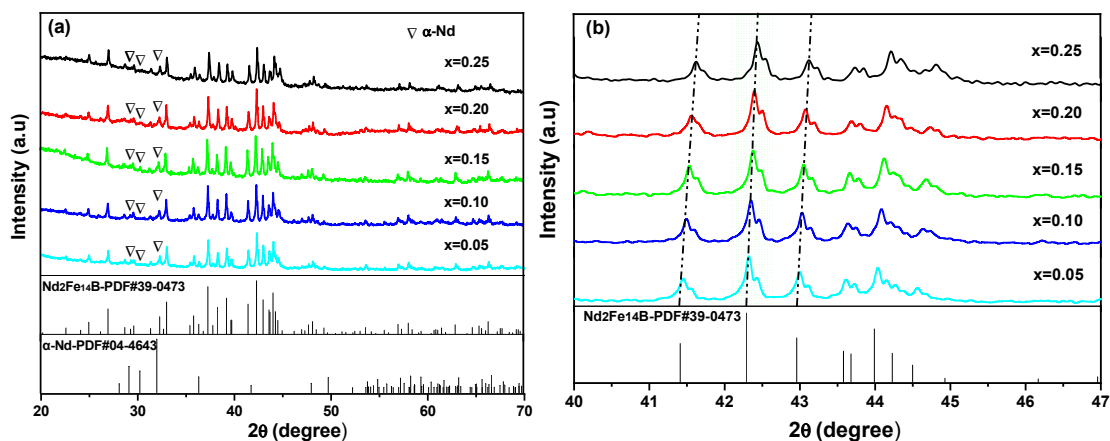


Figure 1. XRD powder patterns (a) and local XRD patterns (b) of $(\text{Nd}_{1-2x}\text{Ce}_x\text{Y}_x)_{14.5}\text{Fe}_{79.3}\text{B}_{6.2}$ alloys annealed at 1173 K for 360 h.

Based on the crystal structure analysis, lattice parameters and cell volumes of $(\text{NdCeY})_2\text{Fe}_{14}\text{B}$ phase in annealed alloys were obtained, as shown in Figure 2. It can be seen that lattice parameters and cell volumes of $(\text{NdCeY})_2\text{Fe}_{14}\text{B}$ phase decrease slightly with the increase of Ce and Y substitutions in annealed alloys because of the replacement of Nd by Ce and Y in the lattice of $\text{Nd}_2\text{Fe}_{14}\text{B}$ phase.

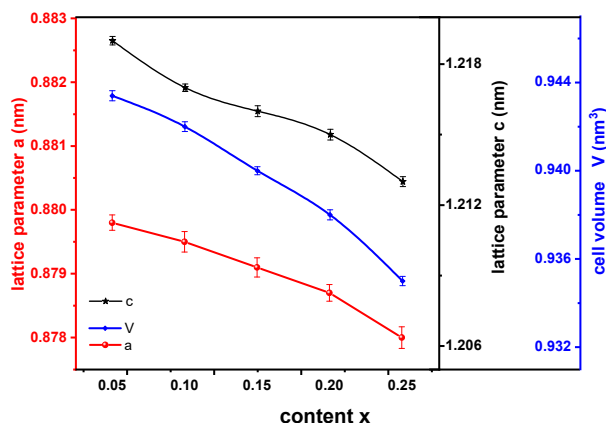


Figure 2. Lattice parameters and cell volumes of $(\text{NdCeY})_2\text{Fe}_{14}\text{B}$ phase in $(\text{Nd}_{1-2x}\text{Ce}_x\text{Y}_x)_{14.5}\text{Fe}_{79.3}\text{B}_{6.2}$ alloys annealed at 1173 K for 360 h.

Figure 3 is the microstructure image of $(\text{Nd}_{1-2x}\text{Ce}_x\text{Y}_x)_{14.5}\text{Fe}_{79.3}\text{B}_{6.2}$ annealed alloys. As can be seen, the microstructure characteristics of the annealed alloys show $(\text{NdCeY})_2\text{Fe}_{14}\text{B}$ phase (gray area) and rich-RE ($\alpha\text{-Nd}$) phase (white area), while the $\alpha\text{-Fe}$ phase was not observed, which is in good agreement with the XRD results. It was found that the volume fraction of the rich-RE ($\alpha\text{-Nd}$) phase (white area) in annealed alloys increases gradually with the increase of Ce and Y substitutions.

Figure 4 is the XRD patterns of $(\text{Nd}_{1-2x}\text{Ce}_x\text{Y}_x)_{14.5}\text{Fe}_{79.3}\text{B}_{6.2}$ melt-spun ribbons. According to the phase analysis of XRD patterns, diffraction peaks in all the ribbons are indexed as the $(\text{NdCeY})_2\text{Fe}_{14}\text{B}$ phase with the tetragonal $\text{Nd}_2\text{Fe}_{14}\text{B}$ -typed structure (space group $P4_2/mnm$), rich-RE ($\alpha\text{-Nd}$) phase, and $\alpha\text{-Fe}$ phase. Especially, the ribbon with $x = 0.25$ has a different phase constitution, which contains additional CeFe_2 phase.

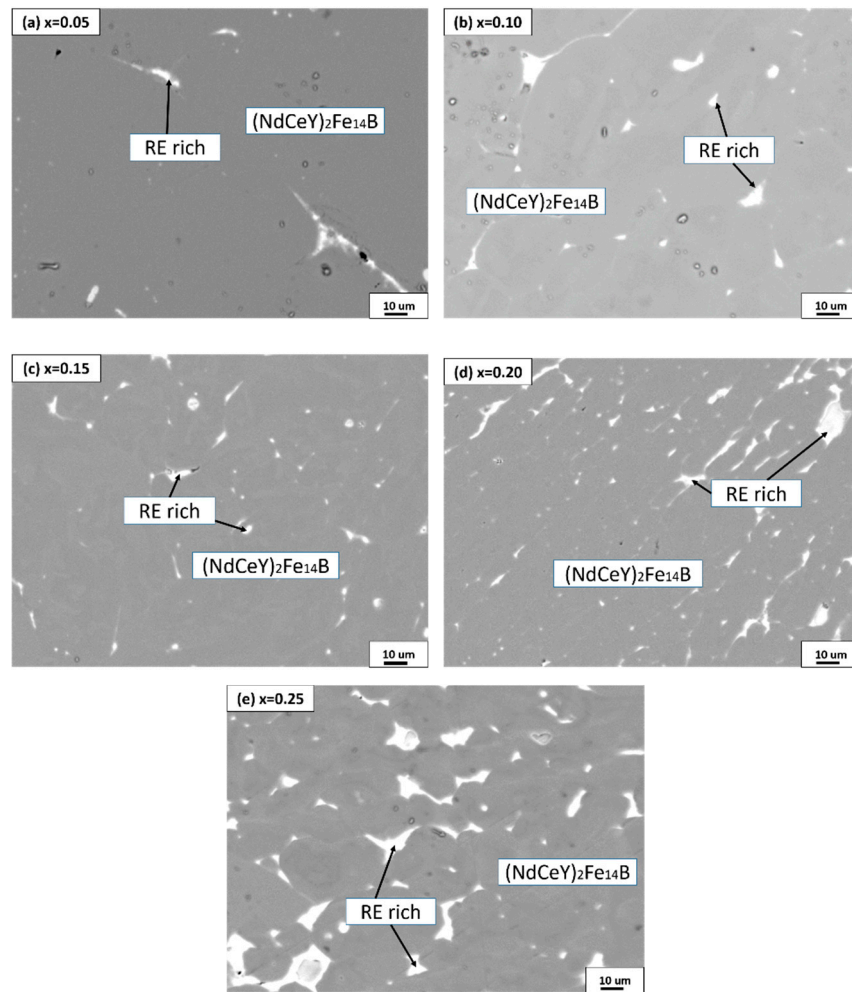


Figure 3. The backscattered electron (BSE) images of $(\text{Nd}_{1-2x}\text{Ce}_x\text{Y}_x)_{14.5}\text{Fe}_{79.3}\text{B}_{6.2}$ alloys annealed 1173 K for 360 h: (a) $x = 0.05$, (b) $x = 0.10$, (c) $x = 0.15$, (d) $x = 0.20$, and (e) $x = 0.25$.

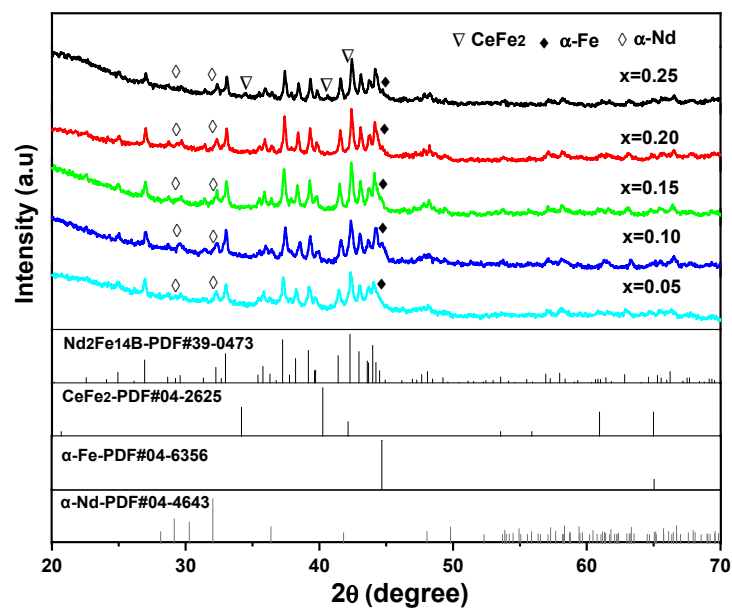


Figure 4. XRD patterns of $(\text{Nd}_{1-2x}\text{Ce}_x\text{Y}_x)_{14.5}\text{Fe}_{79.3}\text{B}_{6.2}$ ($x = 0.05, 0.10, 0.15, 0.20, 0.25$) melt-spun ribbons.

3.2. Magnetic Properties

Figure 5 is the hysteresis loops of $(\text{Nd}_{1-2x}\text{Ce}_x\text{Y}_x)_{14.5}\text{Fe}_{79.3}\text{B}_{6.2}$ melt-spun ribbons. It can be seen that the hysteresis loops show very poor squareness, which could result from the formation of $\alpha\text{-Fe}$ and CeFe_2 phases in the ribbons. With the increase of Ce and Y substitutions, the remanent magnetization (M_r) and saturation magnetization (M_s) of the ribbons decrease monotonically because the intrinsic magnetic properties of $\text{Ce}_2\text{Fe}_{14}\text{B}$ and $\text{Y}_2\text{Fe}_{14}\text{B}$ phases are lower than those of the $\text{Nd}_2\text{Fe}_{14}\text{B}$ phase [35].

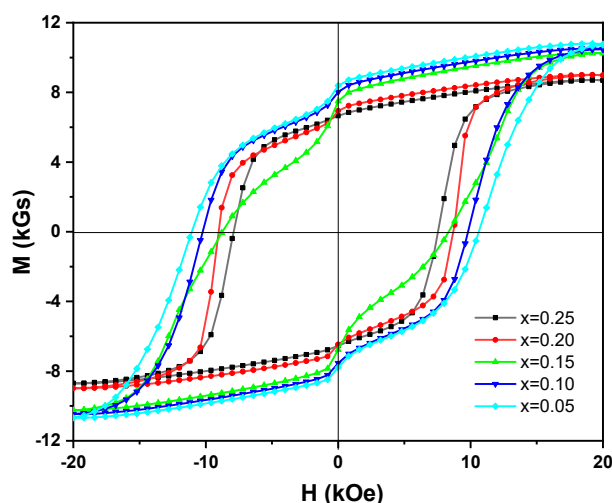


Figure 5. Hysteresis loops of $(\text{Nd}_{1-2x}\text{Ce}_x\text{Y}_x)_{14.5}\text{Fe}_{79.3}\text{B}_{6.2}$ ($x = 0.05, 0.10, 0.15, 0.20, 0.25$) melt-spun ribbons at room temperature.

Based on the hysteresis loops of $(\text{Nd}_{1-2x}\text{Ce}_x\text{Y}_x)_{14.5}\text{Fe}_{79.3}\text{B}_{6.2}$ melt-spun ribbons in Figure 5, the remanence (B_r) and the coercivity (H_{cj}) of the ribbons were obtained, while the maximum magnetic energy product ($(\text{BH})_{\text{max}}$) was determined from the area of the largest rectangle in the second quadrant of B-H curves transformed from the hysteresis loops. Table 1 summarizes magnetic properties of $(\text{Nd}_{1-2x}\text{Ce}_x\text{Y}_x)_{14.5}\text{Fe}_{79.3}\text{B}_{6.2}$ melt-spun ribbons. The remanence (B_r) of $(\text{Nd}_{1-2x}\text{Ce}_x\text{Y}_x)_{14.5}\text{Fe}_{79.3}\text{B}_{6.2}$ melt-spun ribbons are 8.69 kGs, 7.72 kGs, 7.49 kGs, 6.65 kGs, and 6.64 kGs, respectively, while the coercivity (H_{cj}) of the ribbons are 11.04 kOe, 10.21 kOe, 8.75 kOe, 9.01 kOe, and 7.85 kOe, respectively. In general, the remanence (B_r) and the coercivity (H_{cj}) of the ribbons deteriorate gradually with the increase of Ce and Y substitutions, except for the ribbon with $x = 0.15$, in which the coercivity (H_{cj}) is higher than that of the ribbon with $x = 0.10$. The reason for it could result from the inferior magnetic properties of $\text{Ce}_2\text{Fe}_{14}\text{B}$ and $\text{Y}_2\text{Fe}_{14}\text{B}$ phases [35]. Based on the experimental results of the remanence (B_r) and the coercivity (H_{cj}) mentioned above, the maximum magnetic energy product ($(\text{BH})_{\text{max}}$) of the ribbons was determined to be 12.98 MGOe, 10.64 MGOe, 6.86 MGOe, 8.33 MGOe, and 9.06 MGOe, respectively. It was found that $(\text{BH})_{\text{max}}$ of the ribbon with $x = 0.15$ is the smallest due to the poor squareness of the hysteresis loop, while the ribbon with $x = 0.25$ has good magnetic performance ($B_r = 6.64$ kGs, $H_{cj} = 7.85$ kOe, $(\text{BH})_{\text{max}} = 9.06$ MGOe), indicating that magnetic properties of Nd-Ce-Y-Fe-B ribbons could be regulated by alloy composition and phase formation.

Table 1. Magnetic properties of $(\text{Nd}_{1-2x}\text{Ce}_x\text{Y}_x)_{14.5}\text{Fe}_{79.3}\text{B}_{6.2}$ melt-spun ribbons.

Melt-Spun Ribbons $(\text{Nd}_{1-2x}\text{Ce}_x\text{Y}_x)_{14.5}\text{Fe}_{79.3}\text{B}_{6.2}$	B_r (kGs)	H_{cj} (kOe)	$(\text{BH})_{\text{max}}$ (MGOe)	M_r (emu/g)	Remanent Ratio (M_r/M_s)	Squareness
$x = 0.05$	8.69	11.04	12.98	83.71	0.78	0.63
$x = 0.10$	7.72	10.20	10.64	80.06	0.75	0.67
$x = 0.15$	7.49	8.75	6.86	74.83	0.73	0.46
$x = 0.20$	6.65	9.01	8.33	69.27	0.77	0.70
$x = 0.25$	6.64	7.85	9.06	66.43	0.76	0.76

Figure 6 shows the initial magnetization curves and demagnetization curves of $(\text{Nd}_{1-2x}\text{Ce}_x\text{Y}_x)_{14.5}\text{Fe}_{79.3}\text{B}_{6.2}$ melt-spun ribbons. From the shape of the initial magnetization curves in Figure 6a, the magnetization process of the ribbons is staged, and all ribbons are controlled by the nucleation model and the domain wall pinning model. The first and second derivatives of the initial magnetization curves of the ribbons are shown in Figure 6b, which analyze better the pinning field distribution and the magnetization characteristics. As can be seen, the magnetization processes of the ribbons with $x = 0.05, 0.10, 0.20, 0.25$ are mainly controlled by the domain wall pinning model, while the magnetization process of the ribbon with $x = 0.15$ is mainly controlled by the nucleation model. When the magnetic field is 0–2.5 kOe, the dM/dH along with the increase of magnetic field increases and declines rapidly, indicating that the magnetization process of the ribbons is dominated by nucleation at the beginning, which could be due to the existence of α -Fe phase in the ribbons. The α -Fe phase has exchange coupling with the $(\text{NdCeY})_2\text{Fe}_{14}\text{B}$ phase, which promotes the rapid magnetization of the primary phase. With the increase of the magnetic field, the presence of rich-RE phases provides a pinning field in $(\text{Nd}_{1-2x}\text{Ce}_x\text{Y}_x)_{14.5}\text{Fe}_{79.3}\text{B}_{6.2}$ ribbons during the magnetization process, and the magnetization process is mainly dominated by the domain wall pinning. The magnetization of the ribbons would overcome the nailing action of grain boundary to its domain wall. After reaching the critical magnetic field, the magnetization increases sharply to saturation magnetization. The second derivative of the initial magnetization curve has only one extreme point, which indicates that the distribution of the pinning field is relatively uniform. In addition, since the magnetocrystalline anisotropy constants of $\text{Ce}_2\text{Fe}_{14}\text{B}$ and $\text{Y}_2\text{Fe}_{14}\text{B}$ are lower than that of $\text{Nd}_2\text{Fe}_{14}\text{B}$ [35], the strength of the pinning field decreases gradually with the increase of Ce and Y substitutions.

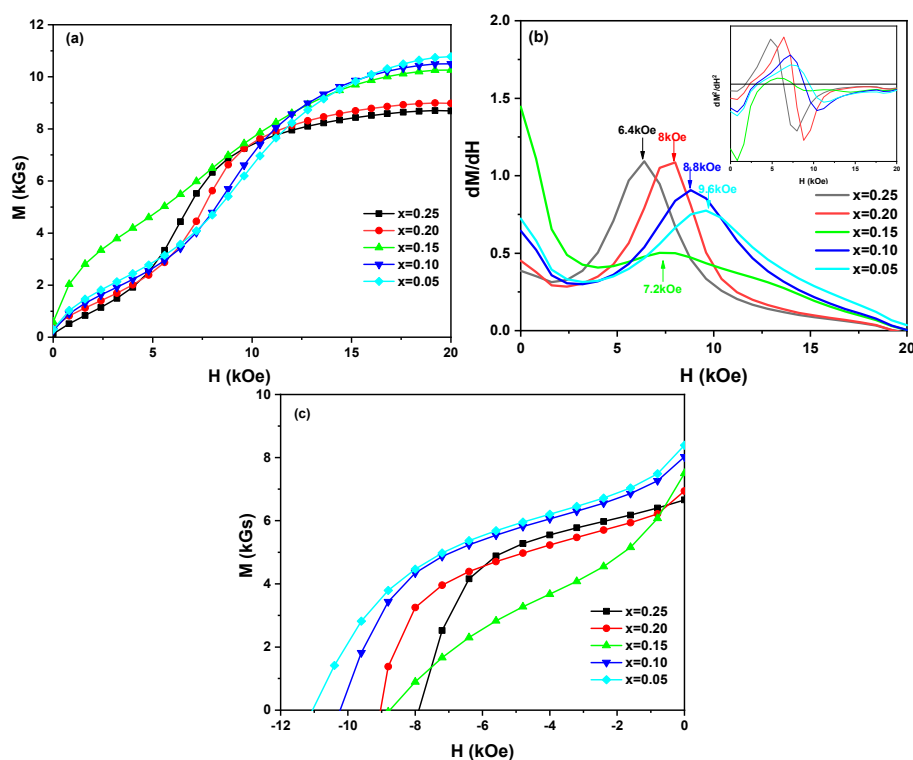


Figure 6. Initial magnetization curves (a), the first and second derivatives of the initial magnetization curve (b), and demagnetization curves (c) of $(\text{Nd}_{1-2x}\text{Ce}_x\text{Y}_x)_{14.5}\text{Fe}_{79.3}\text{B}_{6.2}$ ($x = 0.05, 0.10, 0.15, 0.20, 0.25$) melt-spun ribbons at room temperature.

As shown in Figure 6c, the kinks were observed in the demagnetization curves of the ribbons (except for the ribbon with $x = 0.25$). This phenomenon could result from the formation and uniform distribution of the soft magnetic phase (such as α -Fe and CeFe_2

phases) in the ribbons. In addition, the region of α -Fe and/or CeFe_2 phase would partially exchange-couple to the adjacent $(\text{NdCeY})_2\text{Fe}_{14}\text{B}$ phase, reversing incongruously to present kinks in the demagnetization curves.

4. Conclusions

In this work, phase structure, microstructure, and magnetic properties of $(\text{Nd}_{1-2x}\text{Ce}_x\text{Y}_x)_{14.5}\text{Fe}_{79.3}\text{B}_{6.2}$ ($x = 0.05, 0.10, 0.15, 0.20, 0.25$) alloys were investigated. The following results could be obtained:

- (1) The XRD and SEM results show that $(\text{Nd}_{1-2x}\text{Ce}_x\text{Y}_x)_{14.5}\text{Fe}_{79.3}\text{B}_{6.2}$ annealed alloys contain the $(\text{NdCeY})_2\text{Fe}_{14}\text{B}$ phase with the tetragonal $\text{Nd}_2\text{Fe}_{14}\text{B}$ -typed structure (space group $P4_2/mnm$) and rich-RE (α -Nd) phase. Meanwhile, $(\text{Nd}_{1-2x}\text{Ce}_x\text{Y}_x)_{14.5}\text{Fe}_{79.3}\text{B}_{6.2}$ melt-spun ribbons are composed of $(\text{NdCeY})_2\text{Fe}_{14}\text{B}$ phase, α -Nd phase and α -Fe phase, except for the ribbon with $x = 0.25$, which consists of additional CeFe_2 phase.
- (2) Magnetic measurements show that the B_r and the H_{cj} of $(\text{Nd}_{1-2x}\text{Ce}_x\text{Y}_x)_{14.5}\text{Fe}_{79.3}\text{B}_{6.2}$ ribbons decrease with the increase of Ce and Y substitutions, while the $(\text{BH})_{\text{max}}$ of the ribbons decrease and then increase. The tendency of magnetic properties of the ribbons could result from the co-substitution of Ce and Y for Nd in $\text{Nd}_2\text{Fe}_{14}\text{B}$ phase and different phase formation.
- (3) The H_{cj} of the ribbon with $x = 0.20$ is relatively high to be 9.01 kOe, while the $(\text{BH})_{\text{max}}$ of the ribbon with $x = 0.25$ is still 9.06 MGOe. It indicates that the magnetic performance of Nd-Ce-Y-Fe-B melt-spun ribbons would be regulated through alloy composition and phase formation to fabricate novel Nd-Fe-B magnets with low costs and high performance.

Author Contributions: Conceptualization, Q.K., M.R. and J.W.; methodology, Q.K. and F.D.; formal analysis, S.L.; investigation, Q.K. and M.R.; data curation, Q.Y.; writing—original draft preparation, Q.K. and M.R.; writing—review and editing, M.R. and J.W.; supervision, M.R., Q.Y. and J.W.; project administration, J.W. All authors have read and agreed to the published version of the manuscript.

Funding: This work was supported financially by the National Natural Science Foundation of China (51761008, 51971069), Guangxi Natural Science Foundation (2020GXNSFFA297004, 2016GXNSFDA380015), Guangxi Project of Science and Technology (2017AD23031), and Engineering Research Center of Electronic Information Materials and Devices, Guilin University of Electronic Technology, China (EIMD-AA202004). The authors thank the support from the foundation for Guangxi Bagui scholars and National Undergraduate Training Program for Innovation (201910595016).

Institutional Review Board Statement: Not applicable.

Informed Consent Statement: Not applicable.

Data Availability Statement: Data sharing is not applicable to this article.

Conflicts of Interest: The authors declare no conflict of interest.

References

1. Sagawa, M.; Fujimura, S.; Togawa, N.; Yamamoto, H.; Matsuura, Y. New material for permanent magnets on a base of Nd and Fe. *J. Appl. Phys.* **1984**, *55*, 2083–2087. [[CrossRef](#)]
2. Gutfleisch, O.; Willard, M.A.; Brück, E.; Chen, C.H.; Sankar, S.G.; Liu, J.P. Magnetic materials and devices for the 21st century: Stronger, lighter, and more energy efficient. *Adv. Mater.* **2011**, *20*, 1–22. [[CrossRef](#)]
3. Poudyal, N.; Liu, J.P. Advances in nanostructured permanent magnets research. *J. Phys. D Appl. Phys.* **2013**, *46*, 43001–43023. [[CrossRef](#)]
4. Zhu, M.G.; Li, W.; Wang, J.D.; Zheng, L.Y.; Li, Y.F.; Zhang, K.; Feng, H.; Liu, T. Influence of Ce content on the rectangularity of demagnetization curves and magnetic properties of Re-Fe-B magnets sintered by double main phase alloy method. *IEEE Trans. Magn.* **2014**, *50*, 1–4. [[CrossRef](#)]
5. Li, X.M.; Lu, Z.; Yao, Q.R.; Wei, Q.; Wang, J.; Du, Y.S.; Li, L.; Long, Q.X.; Zhou, H.Y.; Rao, G.H. Thermal stability of high-temperature compound $\text{La}_2\text{Fe}_{14}\text{B}$ and magnetic properties of Nd-La-Fe-B alloys. *J. Alloys Compd.* **2021**, *859*, 157780. [[CrossRef](#)]
6. Rong, M.H.; Ma, J.; Yao, Q.R.; Wang, J.; Rao, G.H.; Zhou, H.Y.; Jin, Z.P. Effect of Ce on phase formation and magnetic properties of $(\text{Nd-Pr})_{2.28}\text{Fe}_{13.58}\text{B}_{1.14}$ melt-spun ribbons. *Mater. Res. Express.* **2020**, *7*, 076101. [[CrossRef](#)]

7. Rong, M.H.; Fu, G.; Yao, Q.R.; Wang, J.; Rao, G.H.; Zhou, H.Y.; Jin, Z.P. Phase structure, microstructure and magnetic properties of (Nd-Ce)_{13.4}Fe_{79.9}B_{6.7} alloys. *J. Supercond. Nov. Magn.* **2020**, *33*, 2737–2744. [[CrossRef](#)]
8. Li, Z.B.; Shen, B.G.; Zhang, M.; Hu, F.X.; Sun, J.R. Substitution of Ce for Nd in preparing R₂ Fe₁₄B nanocrystalline magnets. *J. Alloys Compd.* **2015**, *628*, 325–328. [[CrossRef](#)]
9. Pthank, A.K.; Khan, M.; Gschneidner, K.A., Jr.; Mccallum, R.W.; Zhou, L.; Sun, K.; Dennis, K.W.; Zhou, C.; Pinkerton, F.E.; Kramer, M.J.; et al. Cerium: An unlikely replacement of dysprosium in high performance Nd-Fe-B permanent magnets. *Adv. Mater.* **2015**, *27*, 2663–2667.
10. Pathak, A.K.; Gschneidner, K.A.; Khan, M.; Mccallum, R.W.; Pecharsky, V.K. High performance Nd-Fe-B permanent magnets without critical elements. *J. Alloys Compd.* **2016**, *668*, 80–86. [[CrossRef](#)]
11. Hussain, M.; Zhao, L.Z.; Zhang, C.; Jiao, D.L.; Zhong, X.C.; Liu, Z.W. Composition-dependent magnetic properties of melt-spun La or/and Ce substituted nanocomposite NdFeB alloys. *Phys. B Condensed. Matter.* **2016**, *483*, 69–74. [[CrossRef](#)]
12. Fan, X.D.; Guo, S.; Chen, K.; Chen, R.J.; Lee, D.; You, C.Y.; Yan, A.R. Tuning Ce distribution for high performance Nd-Ce-Fe-B sintered magnets. *J. Magn. Magn. Mater.* **2016**, *419*, 394–399. [[CrossRef](#)]
13. Pei, K.; Lin, M.; Yan, A.R.; Zhang, X. Effects of annealing process on magnetic properties and structures of Nd-Pr-Ce-Fe-B melt-spun powders. *J. Magn. Magn. Mater.* **2016**, *406*, 239–243. [[CrossRef](#)]
14. Jiang, Q.Z.; Zhong, Z.C. Research and development of Ce-containing Nd₂Fe₁₄B-type alloys and permanent magnetic materials. *J. Mater. Sci. Technol.* **2017**, *33*, 1087–1096. [[CrossRef](#)]
15. Zha, L.; Liu, Z.; Chen, H.; Xue, M.Z.; Qiao, G.Y.; Ding, S.L.; Wen, X.; Zhang, M.L.; Lai, Y.F.; Yang, W.Y.; et al. High coercivity Nd-Ce-Fe-B nanostructure ribbons prepared from melt spinning technique. *J. Rare Earths* **2018**, *37*, 1053–1058. [[CrossRef](#)]
16. Wang, L.; Wang, J.; Rong, M.H.; Rao, G.H.; Zhou, H.Y. Effect of wheel speed on phase formation and magnetic properties of (Nd_{0.4}La_{0.6})-Fe-B melt-spun ribbons. *J. Rare Earths* **2018**, *36*, 1179–1183. [[CrossRef](#)]
17. Lei, W.K.; Jiang, Q.Z.; Rehman, S.U.; He, L.K.; Hu, X.J.; Zeng, Q.W.; Tan, Q.L.; Liu, R.H.; Zhong, M.L.; Zhong, Z.C. Effect of La-substitution on microstructure and magnetic property of melt-spun (Nd_{1-x}La_x)₁₃Fe₈₁B₆ alloys. *J. Magn. Magn. Mater.* **2019**, *473*, 155–160. [[CrossRef](#)]
18. Ma, T.Y.; Yan, M.; Wu, K.Y.; Wu, B.; Liu, X.L.; Wang, X.J.; Qian, Z.Y.; Wu, C.; Xia, W.Q. Grain boundary restructuring of multi-main-phase Nd-Ce-Fe-B sintered magnets with Nd hydrides. *Acta Mater.* **2018**, *142*, 18–28. [[CrossRef](#)]
19. Hussain, M.; Zhao, L.Z.; Akram, R.; Ahmad, Z.; Zhang, Z.Y.; Gulzar, A.; Zhong, X.C.; Liu, Z.W. Magnetic properties and exchange interaction of rapidly quenched La or Ce substituted nanocrystalline NdFeB alloys with various compositions. *J. Magn. Magn. Mater.* **2018**, *468*, 141–147. [[CrossRef](#)]
20. Yan, M.; Jin, J.Y.; Ma, T.Y. Grain boundary restructuring and La/Ce/Y application in Nd-Fe-B magnets. *Chin. Phys. B.* **2019**, *28*, 27–56. [[CrossRef](#)]
21. Rehman, S.U.; Song, J.; Jiang, Q.Z.; He, L.K.; Xie, W.C.; Zhong, Z.C. Magnetic properties, phase transition temperature, intergranular exchange interactions and microstructure of Ta-doped Nd-Ce-Fe-B nano ribbons. *J. Supercond. Nov. Magn.* **2020**, *33*, 877–882. [[CrossRef](#)]
22. Jin, J.Y.; Yan, M.; Ma, T.Y.; Li, W.; Liu, Y.S.; Zhang, Z.H.; Fu, S. Balancing the microstructure and chemical heterogeneity of multi-main-phase Nd-Ce-Fe-B sintered magnets by tailoring the liquid-phase-sintering. *Mater. Des.* **2020**, *186*, 108308. [[CrossRef](#)]
23. Zhao, L.Z.; Li, C.L.; Hao, Z.P.; Liu, X.L.; Liao, X.F.; Zhang, J.S.; Su, K.P.; Li, L.W.; Yu, H.Y.; Greneche, J.M.; et al. Influences of element segregation on the magnetic properties in nanocrystalline Nd-Ce-Fe-B alloys. *Mater. Charact.* **2019**, *148*, 208–213. [[CrossRef](#)]
24. Zhang, Y.J.; Ma, T.Y.; Yan, M.; Jian, J.Y.; Liu, X.L.; Xu, F.; Miao, X.F.; Liu, C.Y. Squareness factors of demagnetization curves for multi-main-phase Nd-Ce-Fe-B magnets with different Ce contents. *J. Magn. Magn. Mater.* **2019**, *487*, 165355. [[CrossRef](#)]
25. Pei, K.; Zhang, X.; Lin, M.; Yan, A.R. Effects of Ce-substitution on magnetic properties and microstructure of Nd-Pr-Fe-B melt-spun powders. *J. Magn. Magn. Mater.* **2016**, *398*, 96–100. [[CrossRef](#)]
26. Chen, Z.; Luo, J.; Sui, Y.L.; Guo, Z.M. Effect of yttrium substitution on magnetic properties and microstructure of Nd-Y-Fe-B nanocomposite magnets. *J. Rare Earths* **2010**, *28*, 277–281. [[CrossRef](#)]
27. Tang, W.; Wu, Y.Q.; Oster, N.T.; Dennis, K.W.; Kramer, M.J.; Aderson, I.E.; Maccallum, R.W. Improved energy product in grained aligned and sintered MRE₂Fe₁₄B magnets (MRE = Y + Dy + Nd). *J. Appl. Phys.* **2010**, *107*, 09A728-1–09A728-3.
28. Liu, Z.W.; Qian, D.Y.; Zeng, D.C. Redducting Dy content by Y substitution in nanocomposite NdFeB alloys with enhanced magnetic properties and thermal stability. *IEEE Trans. Magn.* **2012**, *48*, 2797–2799. [[CrossRef](#)]
29. Peng, B.X.; Ma, T.Y.; Zhang, Y.J.; Jin, J.Y.; Yan, M. Improved thermal stability of Nd-Ce-Fe-B sintered magnets by Y substitution. *Sri. Mater.* **2017**, *131*, 11–14. [[CrossRef](#)]
30. Fan, X.D.; Chen, K.; Guo, S.; Chen, R.J.; Lee, D.; Yan, A.R.; You, C.Y. Core-shell Y-substituted Nd-Ce-Fe-B sintered magnets with enhanced coercivity and good thermal stability. *Appl. Phys. Lett.* **2017**, *110*, 172405-1–172405-4. [[CrossRef](#)]
31. Peng, B.X.; Jin, J.Y.; Liu, Y.S.; Zhang, Z.H.; Yan, M. Effects of (Nd, Pr)-Hx addition on the coercivity of Nd-Ce-Y-Fe-B sintered magnet. *J. Alloys Compd.* **2019**, *772*, 656–662. [[CrossRef](#)]
32. Zheng, M.; Fang, Y.K.; Song, L.W.; Han, R.; Zhu, M.G.; Li, W. Magnetic properties and structures of Y-substituted Nd-Y-Fe-B melt-spun ribbons. *Rare Met.* **2018**. [[CrossRef](#)]
33. Liao, S.C.; Ding, G.F.; Zheng, B.; Shu, Z.T.; Chen, R.J.; Yan, A.R.; Guo, S.; Pan, J. Influences of element distribution on the magnetic properties in the (PrNd)-(YCe)-Fe-B sintered magnets. *J. Magn. Magn. Mater.* **2020**, *497*, 165901. [[CrossRef](#)]

-
34. Zhang, C.H.; Luo, Y.; Yu, D.B.; Quan, N.T.; Wu, G.Y.; Dou, Y.K.; Hu, Z.; Wang, Z.L. Permanent magnetic properties of Nd-Fe-B melt-spun ribbons with Y substitution. *Rare Met.* **2020**, *39*, 55–61. [[CrossRef](#)]
 35. Herbst, J.F. R₂Fe₁₄B materials: Intrinsic properties and technological aspects. *Rev. Mod. Phys.* **1991**, *63*, 819–898. [[CrossRef](#)]